

Hyperon-nucleon single-particle potentials with low-momentum interactions

H. Ćapo,^{1,*} B.-J. Schaefer,^{2,†} and J. Wambach^{1,3}

¹*Institut für Kernphysik, TU Darmstadt, Schloßgartenstr. 9, D-64289 Darmstadt, Germany*

²*Institut für Physik, Karl-Franzens-Universität Graz, Universitätsplatz 5, A-8010 Graz, Austria*

³*Gesellschaft für Schwerionenforschung mbH, Planckstr. 1, D-64291 Darmstadt, Germany*

(Dated: August 9, 2021)

Single-particle potentials in Hartree-Fock approximation for different hyperon-nucleon (YN) channels are calculated in the framework of the effective low-momentum YN interaction $V_{\text{low } k}$. In contrast to the nucleon-nucleon interaction, the available experimental data for the YN interaction are scarce. As a consequence no unique YN low-momentum potential $V_{\text{low } k}$ can be predicted from the various bare potentials. The resulting momentum- and density-dependent single-particle potentials for several different bare OBE models and for chiral effective field theory are compared to each other.

PACS numbers: 21.65.-f, 13.75.Ev, 21.30.Fe

I. INTRODUCTION

The understanding of the hyperon-nucleon (YN) interaction is essential to the physics of nuclear systems with strangeness and to the octet of the lightest baryons. Furthermore, since e.g. the core of neutron stars may contain a high fraction of hyperons a deeper knowledge of the YN interaction is also important for astrophysical issues. In recent years, an increased interest in exploring nuclear systems with strangeness, especially multi-strange nuclear systems, becomes apparent. The YN interaction becomes relevant not only when the properties of simple hypernuclei, double strange hypernuclei but also when the production of hyperfragments in relativistic heavy-ion collisions are studied. It also strongly influences the composition and behavior of dense nuclear matter. For an recent overview of hypernuclear physics see [1].

Unfortunately, the details of the YN interaction are known very poorly. On the one hand, there exist only a very limited amount of scattering data from which one could construct high-quality YN potentials based on meson-exchange. The existing data do not constrain the potentials sufficiently. On the other hand, theoretical analyses, especially for many-body systems, do not seem to produce unambiguous results [2, 3]. For example, this uncertainty is immediately demonstrated in that six different parameterizations of the Nijmegen YN potentials fit equally well the scattering data but produce very different scattering lengths, see e.g. [4]. In order to improve the reliability of available hyperon-nucleon and even hyperon-hyperon potentials forthcoming experiments at the planned J-PARC and FAIR facilities are indispensable. Recently, first lattice QCD simulations on the YN interaction have been performed [5]. In [6] the findings on the lattice concerning some aspects of ΛN scattering are confronted with results of the chiral effective field theory (χ EFT).

For the nucleon-nucleon interaction a unique low-momentum effective potential is obtained [7]. This uniqueness is lost in the YN case due to the less constraint bare potentials. Given that there are significant differences between various YN potentials it will be interesting to see how those differences reflect themselves in the hyperon single-particle potentials.

In this work we therefore wish to compare various YN potentials and determine their similarities and differences in a dense baryonic medium. For this purpose we calculate the YN single-particle potentials and compare different low-energy scattering results. The potentials are obtained in a Hartree-Fock approximation with an effective low-momentum YN potential $V_{\text{low } k}$. The $V_{\text{low } k}$ is constructed from several bare YN potentials [8, 9]. Since we work with isospin-symmetric nuclear matter, which contains no hyperons we can neglect the hyperon-hyperon (YY) interaction. This is advantageous since the YY interaction is even less known and constrained than the YN interaction. It has been recently shown that in the construction of the YY interaction, at leading order χ EFT, only one additional operator, which is not present in the YN interaction, appears. The strength of this operator can be roughly estimated from existing data on double hypernuclei [10].

The outline of the paper is as follows: In the next Section we first introduce the definition and formalism of the effective low-momentum potential $V_{\text{low } k}$ for the YN interaction. The $V_{\text{low } k}$ is obtained as a solution of a renormalization group equation, which needs bare YN potentials as initial condition. We introduce and discuss in the following some properties of the bare YN potentials, used in this work and present some low-energy scattering quantities. The following section, Sec. III, is devoted to the calculation of the single-particle potentials in the Hartree-Fock approximation. Results for symmetric nuclear matter, the partial-wave contribution to the single-particle potentials and a comparison to other approaches are shown. Finally, we end in Sec. IV with a summary and conclusion.

*E-Mail: haris@crunch.ikp.physik.tu-darmstadt.de

†E-Mail: bernd-jochen.schaefer@uni-graz.at

II. LOW-MOMENTUM INTERACTIONS

We consider hyperons ($Y = \Lambda, \Sigma^+, \Sigma^0, \Sigma^-$) with strangeness $S = -1$ in an infinite system of nucleons N composed of equal numbers of protons p and neutrons n . We consider densities around nuclear saturation density $\rho_0 \approx 0.16 \text{ fm}^{-3}$ corresponding to a Fermi momentum $k_{F,0} = 1.35 \text{ fm}^{-1}$. The electromagnetic interaction is switched off. There exists only a very limited amount of scattering data with which one can construct phenomenological potentials. These potentials are used as initial condition for solving RG equations, which lead to effective low-momentum YN interactions $V_{\text{low } k}$'s. From these different effective $V_{\text{low } k}$'s we finally calculate the single-particle potential for the Λ -hyperon. We start with a brief review of the construction of the low-momentum YN interaction. Details for several bare YN potentials within the RG framework used here can be found in Refs. [8, 9].

A. Construction of $V_{\text{low } k}$

The starting point for the construction of the $V_{\text{low } k}$ is the half-on-shell T -matrix, $T(q', q; E_y)$, which is determined by the nonrelativistic Lippmann-Schwinger equation in momentum space. The on-shell energy is denoted by E_y while q', q are relative momenta between a hyperon and nucleon. An effective low-momentum $T_{\text{low } k}$ -matrix is then obtained by introducing a cutoff Λ in the Lippmann-Schwinger kernel thus integrating the intermediate-state momenta up to this cutoff. At the same time, the bare potential in the coupled-channel partial-wave Lippmann-Schwinger equation are replaced with the corresponding low-momentum potential $V_{\text{low } k}$,

$$T_{\text{low } k, y' y}^{\alpha' \alpha}(q', q; E_y) = V_{\text{low } k, y' y}^{\alpha' \alpha}(q', q) + \frac{2}{\pi} \sum_{\beta, z} P \int_0^\Lambda dl l^2 \frac{V_{\text{low } k, y' z}^{\alpha' \beta}(q', l) T_{\text{low } k, z y}^{\beta \alpha}(l, q; E_y)}{E_y(q) - E_z(l)}. \quad (1)$$

The labels y, z indicate the particle channels, e.g. $y = YN$ and α, β denote the partial waves, e.g. $\alpha = LSJ$ where L is the angular, J the total momentum and S the spin. In Eq. (1) the energies are given by

$$E_y(q) = M_y + \frac{q^2}{2\mu_y}, \quad (2)$$

with the reduced mass $\mu_y = M_Y M_N / M_y$ and total mass $M_y = M_Y + M_N$ of the hyperon M_Y and the nucleon M_N .

Finally, the effective low-momentum $V_{\text{low } k}$ is defined by the requirement that the T -matrices are equivalent for all momenta below this cutoff

$$T^{\alpha' \alpha}(q', q; E) = T_{\text{low } k}^{\alpha' \alpha}(q', q; E), \quad q', q \leq \Lambda.$$

The $V_{\text{low } k}$ thus obtained is non-hermitian but nevertheless phase-shift equivalent hermitian low-momentum YN interactions can be obtained. Since the low-momentum T -matrix, $T_{\text{low } k}$ must be cutoff-independent, i.e. $dT_{\text{low } k}/d\Lambda = 0$ an RG flow equation for $V_{\text{low } k}$

$$\frac{dV_{\text{low } k}(k', k)}{d\Lambda} = \frac{2}{\pi} \frac{V_{\text{low } k}(k', \Lambda) T(\Lambda, k; \Lambda^2)}{1 - k^2/\Lambda^2} \quad (3)$$

can immediately be derived. Instead of solving this flow equation with standard numerical methods (e.g. Runge-Kutta method) directly, the so-called ALS iteration method, pioneered by Andreozzi, Lee and Suzuki, is used [11, 12, 13]. This iteration method is based on a similarity transformation and its solution corresponds to solving the flow equation. Details about the convergence of the ALS iteration method, applied for the coupled channel YN interaction, can be found in [8]. For the hyperon-nucleon interaction with strangeness $S = -1$ two different basis systems, the isospin and the particle basis of the bare potentials are available. We will use the latter.

Furthermore, in our investigations only the diagonal elements of the matrices are needed. Therefore, we will shorten our notation further and introduce the abbreviation $V_{y' y}^{\alpha' \alpha}(q', q) \rightarrow V_y^{\alpha}(q)$ for all diagonal quantities.

B. Bare potentials

In order to solve the flow equation (3) a bare potential as initial condition for the flow has to be chosen. In this work several initial YN potentials, the original Nijmegen soft core model NSC89 [14], the series of models NSC97a-f [4] also by the Nijmegen group and a recent model proposed by the Jülich group [15], labeled as J04 in the following, are used. All these models are formulated in the conventional meson-exchange (OBE) framework. They involve a set of parameters, which have to be determined from the available scattering data. These are the coupling constants of the corresponding baryon-baryon-meson vertices and cutoff parameters for the vertex form factors. Due to the scarce YN scattering data base these parameters cannot be precisely fixed in contrast to the NN interaction, where a lot of scattering data are available. In order to construct consistently conventional OBE models for the YN interaction one usually assumes flavor $SU(3)$ constraints or G -parity arguments on the coupling constants, and in some cases even the $SU(6)$ symmetry of the quark model and adjusts their size by fits to NN data. The major conceptual difference between the various conventional OBE models consists in the treatment of the scalar-meson sector, which plays an important role in any baryon-baryon interaction at intermediate ranges. In contrast to the pseudoscalar and vector meson sectors it is still an open issue who are the actual members of the lowest-lying scalar-meson $SU(3)$ multiplet, what are the masses of the exchange particles and how, if at all, the relations for the coupling

constants, obtained by $SU(3)$ flavor symmetry, should be applied. For example, in the older versions of the YN models by the Jülich group [16, 17] a fictitious σ meson with a mass of roughly 550 MeV, arising from correlated $\pi\pi$ exchange was introduced. The coupling strength of this meson to the baryons was treated as a free parameter and finally fitted to the data. However, in the novel Jülich YN potential [15] a microscopic model of the correlated $\pi\pi$ and $K\bar{K}$ exchange is established in order to fix the contributions in the scalar σ - and vector ρ -channel. This new model incorporates also the common one-boson exchange parts of the lowest pseudoscalar and vector meson multiplets. The corresponding coupling constants are determined by $SU(3)$ flavor symmetry and the so-called $F/(F+D)$ ratios are fixed by the pseudoscalar and vector meson multiplets by invoking $SU(6)$ symmetry.

In the Nijmegen YN models, NSC89 [14], NSC97 [4] and in the recently extended soft-core model for strangeness $S = -2$ ESC04 [18, 19] the interaction is generated by a genuine scalar $SU(3)$ nonet meson exchange. Besides the scalar-meson nonet two additional nonets, the pseudoscalar and vector $SU(3)$ flavor nonets are considered in all Nijmegen models. In addition, Pomeron exchange is also included, which provides additional short-range repulsion. Nevertheless, there are a few conceptual differences in the various Nijmegen models. In the NSC97 models the strength parameter for the spin-spin interaction the magnetic $F/(F+D)$ ratio is left as an open parameter and takes six different values in between a range of 0.4447 to 0.3647 for the six different models NSC97a-f. In the original Nijmegen SC89 model this parameter is constrained by weak-decay data. Furthermore, the NSC97 models include additional $SU(3)$ flavor breaking, which is based on the so-called 3P_0 model [20].

The predictions of the above mentioned models can be compared with an another approach, the so-called chiral effective field theory (χ EFT) to nuclear interactions, which is based on chiral perturbation theory (for recent reviews see e.g. [21, 22, 23]). The major benefit of the χ EFT is the underlying power counting scheme, proposed by Weinberg [24, 25], that allows to improve the calculations systematically by going to higher orders in the expansion. In addition, higher two- and three-body forces can be derived consistently in this framework. Furthermore, the effective potential is explicitly energy independent in contrast to the original Weinberg scheme.

Within χ EFT the NN interaction has been analyzed recently to a high precision (N^3 LO) [26]. To leading order (LO) the NN potential is composed of pion exchanges and a series of contact interactions with an increasing number of derivatives which parameterize the singular short-range part of the NN force. In order to remove the high-energy components of the baryonic and pseudoscalar meson fields a cutoff Λ dependent regulator function in the Lippmann-Schwinger (LS) equation is introduced. With this regularized LS equation observable quantities can be calculated. The cutoff range is limited from below by the mass of the pseudoscalar exchange

mesons. Note, that in conventional meson-exchange models the LS equation is not regularized and convergence is achieved by introducing form factors with corresponding cutoff masses for each meson-baryon-baryon vertices.

So far, the YN interaction has not been investigated in the context of the χ EFT as extensively as the NN interaction. A recent application to the YN interaction by the Jülich group can be found e.g. in [27]. Analogous to the NN case, the YN potential, obtained in LO χ EFT, and consists of four-baryon contact terms and pseudoscalar meson (Goldstone boson) exchanges, which are all related by $SU(3)_f$ symmetry. For the YN interaction typical values for the cutoff lie in the range between 550 and 700 MeV (see e.g. [26]). At LO χ EFT and for a fixed cutoff Λ and pseudoscalar $F/(F+D)$ ratio there are five free parameters. The remaining interaction in the other YN channels are then determined by $SU(3)_f$ symmetry. A next-to-leading order (NLO) χ EFT analysis of the YN scattering and of the hyperon mass shifts in nuclear matter was performed in [28]. However, in this analysis the pseudoscalar meson-exchange contributions were not taken into account explicitly but the YN scattering data could be described successfully for laboratory momenta below 200 MeV using 12 free parameters. One ambiguity in this approach is the value of the η coupling which is identified with the octet η_8 meson coupling and not with the physical η meson. The influence of this ambiguity on the data description can be disregarded [29].

Since there are scarce YN scattering data available, it has not been possible yet to determine uniquely the spin structure of the YN interaction. Nevertheless, all of the above mentioned OBE models are consistent with the measured YN scattering observables. In addition, all of these potentials include the $\Lambda N - \Sigma N$ conversion process.

C. Low-energy scattering

In order to obtain further insight into the separation of scales for the evolution of the low-momentum $V_{\text{low } k}$ we investigate its cutoff dependence. A common feature of all YN potentials is the long-range one-pion exchange (OPE) tail. In general, the RG decimation eliminates the short-distance part of the bare potential and preserves the model-independent impact of the high-momentum components on low-momentum observables. In this sense, the ambiguities associated with the unresolved short-distance parts of the interaction disappear and a universal low-momentum YN interaction $V_{\text{low } k}$ can be constructed from phase shift equivalent bare YN potentials.

The mentioned hierarchy of scales can be seen e.g. in the $\Sigma^- n$ channel, see Fig. 1. The $V_{\text{low } k}$ matrix elements for vanishing momenta are shown as a function of the cutoff Λ for the 1S_0 partial wave. When Λ is decreased, the resulting $V_{\text{low } k}$ becomes more and more attractive. For

1S_0 and a cutoff $\Lambda \sim 500 - 250$ MeV $V_{\text{low } k}$ becomes cutoff independent. Decreasing the cutoff further below the 2π exchange threshold, which corresponds to a $k \approx 280$ MeV, the cutoff insensitivity disappears since the pion contributions are finally integrated out.

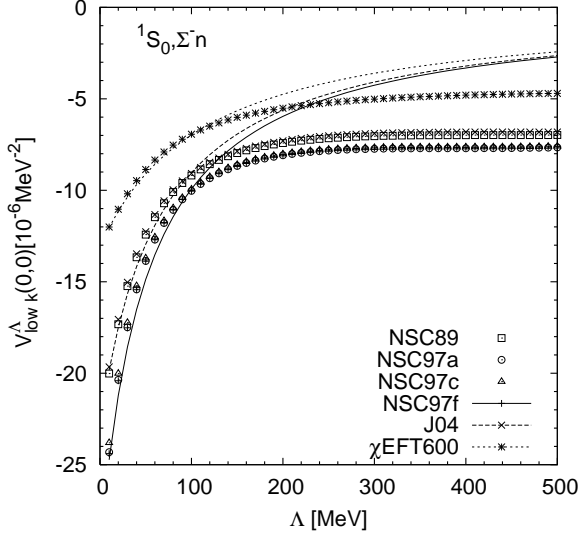


FIG. 1: $V_{\text{low } k}^\Lambda(0)$ in 1S_0 partial wave for various bare potentials as a function of the cutoff Λ in the Σ^-n channel. Prediction from effective range theory (lines) are added.

In the opposite direction, i.e. for $\Lambda \rightarrow \infty$ no fluctuations have been integrated and $V_{\text{low } k}$ tends to the bare potential.

The limit $\Lambda \rightarrow 0$ of $V_{\text{low } k}$ should yield the scattering length. In the limit of small cutoffs an analytic solution obtained in the framework of the effective theory, see [30], is given by the expression

$$V_y(0) = \left[2\frac{\mu_y}{a_0} - 2\frac{\Lambda}{\pi} \right]^{-1} \quad \text{for} \quad \Lambda \rightarrow 0, \quad (4)$$

where we have simplified our notation in an obvious manner. Here, the scattering length a_0 is needed as input, which we have calculated in the standard effective range approximation directly from the T -matrix for the 1S_0 channel from the $V_{\text{low } k}$. In this approximation the T -matrix for $q \leq \Lambda$ can be expanded as

$$q \cot \delta_0 = -\frac{1}{2\mu_y T_y(q, q; q^2)} = -\frac{1}{a_0} + \frac{1}{2}r_0 q^2, \quad (5)$$

where r_0 is the effective range. The results for all different YN flavor channels and for all bare OBE potentials and the χ EFT potential used in this work with cutoffs between 550 and 700 MeV are listed in Tab. I for the scattering length a_0 in units of fm and in Tab. II for the effective range r_0 also in units of fm.

As can be seen from Fig. 1 there is good agreement for small cutoff values Λ between the analytical expansion and the full $V_{\text{low } k}$ solution obtained from the flow equation.

	Λp	Λn	$\Sigma^0 p$	$\Sigma^0 n$	$\Sigma^+ p$	$\Sigma^+ n$	$\Sigma^- p$	$\Sigma^- n$
NSC97a	-0.71	-0.76	-2.46	-1.74	-6.06	-0.04	0.41	-6.13
NSC97b	-0.90	-0.96	-2.47	-1.72	-5.98	-0.04	0.41	-6.06
NSC97c	-1.20	-1.28	-2.41	-1.70	-5.90	-0.03	0.41	-5.98
NSC97d	-1.70	-1.82	-2.38	-1.68	-5.82	-0.03	0.41	-5.89
NSC97e	-2.10	-2.24	-2.38	-1.68	-5.82	-0.03	0.41	-5.90
NSC97f	-2.51	-2.68	-2.45	-1.74	-6.07	-0.05	0.42	-6.16
NSC89	-2.70	-2.72	-2.12	-1.57	-4.79	-0.09	0.23	-4.85
J04	-2.14	-2.11	-2.24	-1.63	-4.68	-0.18	0.04	-4.75
χ EFT550	-1.80	-1.79	-1.76	-1.15	-3.82	0.12	0.31	-3.88
χ EFT600	-1.80	-1.80	-1.25	-0.92	-2.70	0.10	0.20	-2.72
χ EFT650	-1.80	-1.80	-1.43	-1.02	-3.06	0.09	0.21	-3.10
χ EFT700	-1.80	-1.80	-1.50	-1.07	-3.19	0.06	0.20	-3.24

TABLE I: Scattering lengths a_0 of $V_{\text{low } k}$ for different flavor channels in units of fm for the 1S_0 partial wave.

	Λp	Λn	$\Sigma^0 p$	$\Sigma^0 n$	$\Sigma^+ p$	$\Sigma^+ n$	$\Sigma^- p$	$\Sigma^- n$
NSC97a	5.87	6.12	4.58	0.60	3.28	-6602	24.8	3.27
NSC97b	4.93	5.10	4.68	0.59	3.29	-8491	25.0	3.28
NSC97c	4.11	4.23	4.79	0.57	3.30	-10670	25.4	3.29
NSC97d	3.46	3.53	4.91	0.54	3.30	-17115	25.4	3.29
NSC97e	3.19	3.24	4.90	0.52	3.29	-17326	25.2	3.29
NSC97f	3.03	3.09	4.60	0.51	3.25	-6341	24.1	3.24
NSC89	2.86	2.98	5.76	0.74	3.35	-1478	58.0	3.33
J04	2.93	3.09	3.76	1.04	3.32	-329	1232.0	3.30
χ EFT550	1.73	1.84	6.10	-2.96	2.70	-825	34.1	2.68
χ EFT600	1.77	1.88	5.32	-2.12	3.40	-780	10.2	3.39
χ EFT650	1.75	1.86	5.10	-2.28	3.08	-1210	27.6	3.05
χ EFT700	1.74	1.86	4.91	-2.17	2.97	-2450	34.8	2.95

TABLE II: Effective range r_0 . Labeling is the same as in Tab. I.

Unfortunately, no general quantitative conclusion can be drawn from Tab. I and Tab. II due to the bad experimental situation for the YN data. The YN interaction is yet largely unknown. However, agreement of the scattering length of all NSC97 potentials except for the Λp and Λn channels is found. This deviation is related to the different fits of the magnetic $F/(F + D)$ ratio in the Nijmegen potentials [4]. The remaining two potentials, NSC89 and J04, have different but comparable values to those of the NSC97 ones. Unfortunately, the difference between these potentials and the χ EFT potential is large.

Fig. 2 shows the same matrix element as in Fig. 1 but for the 3S_1 partial wave. Unlike to the 1S_0 channel, $V_{\text{low } k}$ for the 3S_1 channel is still cutoff dependent. This can be traced back to the different short-range behavior of the two channels. In the 1S_0 channel the potential has an strongly repulsive core while in the 3S_1 channel the short-distance part is strongly attractive. Hence, dur-

ing the RG decimation towards smaller cutoff values, the potential gets more and more attractive.

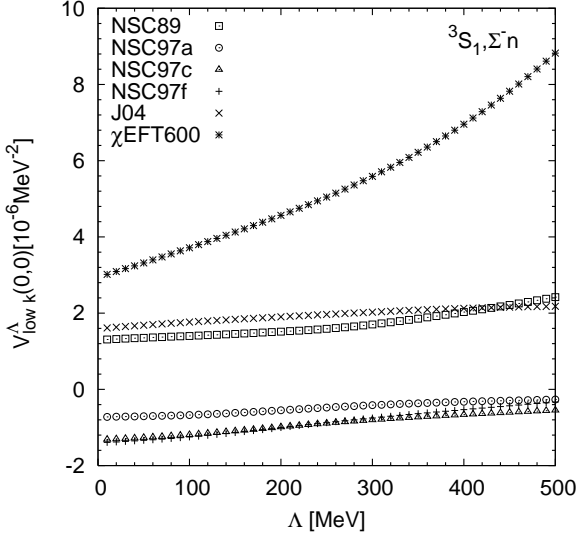


FIG. 2: $V_{\text{low } k}^{\Lambda}(0)$ similar to Fig. 1 for the 3S_1 channel.

III. SINGLE-PARTICLE POTENTIALS

Generally, the single-particle potential $U(p)$ is defined as the diagonal part in spin and isospin space of the proper self-energy for the single-particle Green's function. In the Hartree-Fock approximation for a uniform system it represents the first-order the interaction energy of a particle with incoming momentum p and given spin and isospin with the filled Fermi sea. For the YN interaction the hyperon-nucleon single-particle potential $U_Y(p)$ describes the behavior of the incoming hyperon Y with momentum p in the nuclear medium, i.e. its interaction with a filled Fermi sea of nucleons. The ground-state energy of nuclear matter in first approximation is then obtained by integrating $U(p)$ over the incoming momentum, spin and isospin and adding the kinetic energy. Pictorially, the ground-state energy is represented by closed Goldstone diagrams. By cutting one line, symbolizing the hyperon propagator, in each corresponding Goldstone diagram the $U_Y(p)$ is obtained.

In the following, the calculation of the momentum- and density-dependent $U_Y(p)$ in the Hartree-Fock approximation is presented for symmetric nuclear matter.

A. Hartree-Fock approximation

The single-particle potential $U_Y(p)$ for a hyperon with momentum $p = |\vec{p}|$ is obtained from the diagonal elements of the low-momentum potential matrix, $V_y^{\alpha}(q)$, where the labeling introduced in Eq. (1) has been used.

In a plane-wave basis it splits into two terms, the (direct) Hartree- and the (exchange) Fock-term [31].

$$V_y^{\alpha}(q) = V_y^{\alpha}(q)|_{\text{direct}} + (-1)^{L+S} V_y^{\alpha}(q)|_{\text{exchange}} . \quad (6)$$

Since the low-momentum potential is given in the partial-wave basis we perform a change of basis with the result

$$U_Y(p) = \sum_{\alpha, M_S, M_L} f^{\alpha} \sum_N \int_{t_{\min}}^{t_{\max}} dt P_{LM_L}^2(t) \int_{q_{\min}}^{q_{\max}} dq q^2 V_y^{\alpha}(q) , \quad (7)$$

where $\vec{q} = (M_Y \vec{k} - M_N \vec{p})/M_Y$ denotes the relative momentum between the nucleon \vec{k} and hyperon momentum \vec{p} . The $P_{LM_L}(t)$ are the associated Legendre polynomials of the first kind with the argument $t = \hat{\vec{p}} \cdot \hat{\vec{q}}$, where the hat labels an unit vector. The quantity f^{α} is the short-hand notation for the square of the Clebsch-Gordon coefficients

$$f^{\alpha} = \left(\begin{array}{cc|c} L & S & J \\ M_L & M_S & M_J \end{array} \right)^2 \frac{2L+1}{2\pi} \frac{(L-M_L)!}{(L+M_L)!} , \quad (8)$$

and the M_J , M_L and M_S are the corresponding projections of the total J , angular momentum L and spin S , respectively.

The integration boundaries of $U_Y(p)$ in Eq. (7) are derived in the following: For vanishing temperature the momentum of the nucleon \vec{k} is restricted by the Fermi momentum \vec{k}_F , i.e. $0 \leq k \leq k_F$, and k_F is directly related to the proton or neutron density ρ_N via

$$k_F^3 = 3\pi^2 x_N \rho_B . \quad (9)$$

Here $x_N = \rho_N/\rho_B$ describes the ratio between the proton or neutron and total baryon density. The inequality $0 \leq k \leq k_F$ can be reformulated as

$$M_Y^2 q^2 + M_N^2 p^2 + 2M_Y M_N q p t - M_Y^2 k_F^2 \leq 0$$

which has the solution for the relative momentum q

$$q^-(k_F, p, t) \leq q \leq q^+(k_F, p, t)$$

with the definitions

$$q^{\pm}(k_F, p, t) = \frac{M_N}{M_Y} \left[p \cdot t \pm \sqrt{\frac{M_Y^2}{M_N^2} k_F^2 - p^2(1-t^2)} \right] . \quad (10)$$

Since the relative momentum q is a real quantity this further constrains the integration variable t to

$$t \geq \sqrt{1 - \left(\frac{M_Y}{M_N} \frac{k_F}{p} \right)^2} \quad (11)$$

which is only valid if the hyperon momentum is $p \geq \frac{M_Y}{M_N} k_F$. In this case this finally determines the integration limits as

$$t_{\min} = \sqrt{1 - \left(\frac{M_Y}{M_N} \frac{k_F}{p} \right)^2} ; \quad t_{\max} = 1 ; \\ q_{\min} = q^-(k_F, p, t) ; \quad q_{\max} = q^+(k_F, p, t) \quad (12)$$

because the modulus of t is always smaller or equal one.

For the case that the hyperon momenta $p \leq \frac{M_Y}{M_N} k_F$ the functions $q^\pm(k_F, p, t)$ are always real which then yield the integration limits

$$\begin{aligned} t_{min} &= -1 & ; & \quad t_{max} = 1 ; \\ q_{min} &= 0 & ; & \quad q_{max} = q^+(k_F, p, t) . \end{aligned} \quad (13)$$

In Fig. 3 the integration limit functions q^\pm are shown as a function of t for three different choices of the hyperon momentum ($p < \frac{M_Y}{M_N} k_F, p > \frac{M_Y}{M_N} k_F, p = \frac{M_Y}{M_N} k_F$) and a fixed k_F .

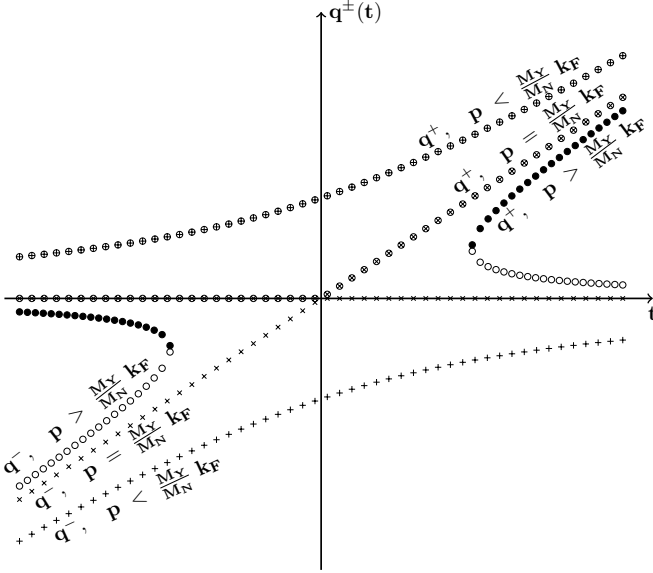


FIG. 3: $q^\pm(k_F, p, t)$ as function of t for different choices of p and fixed k_F .

Thus, the integration limits are known analytically and finally the $U_Y(p)$ are calculated via Eq. (7) numerically with standard integration methods.

B. Symmetric nuclear matter

For symmetric nuclear matter the ratio in Eq. (9) has to be fixed to $x_N = 1/2$. As an example, the numerical solution of Eq. (7) for the full momentum and density dependent single-particle potential of the Λ hyperon with momenta up to 500 MeV and nuclear densities up to $6\rho_0$ is shown in Fig. 4 where as bare potential for the underlying $V_{\text{low } k}$ calculation the NSC97f model of the Nijmegen group has been used. One sees that with increasing density, the momentum dependence becomes stronger, indicating that the effective mass becomes lower for larger densities.

Similarly, Fig. 5 shows the full momentum and density dependence of the Σ^- potential in symmetric nuclear matter based on the NSC97f potential. Here, the slope of the momentum dependence is less pronounced, which

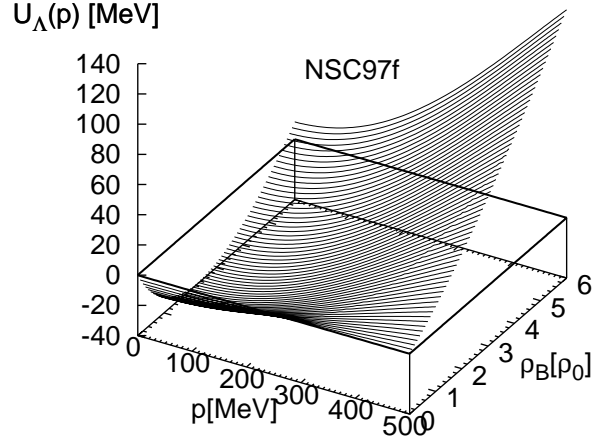


FIG. 4: Momentum and density dependence of $U_\Lambda(p)$ for symmetric nuclear matter. As bare potential the NSC97f was used.

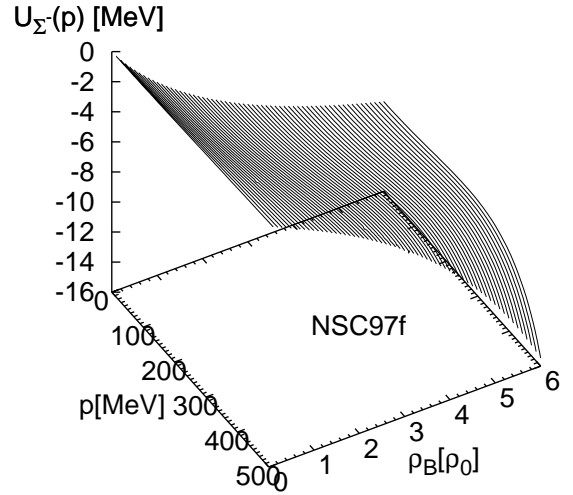


FIG. 5: Similar to Fig. 4 for $U_{\Sigma^-}(p)$.

leads to a weaker density dependent effective mass. However, unlike to the Λ case, the curvature becomes negative at higher densities leading to an larger effective mass than the bare mass.

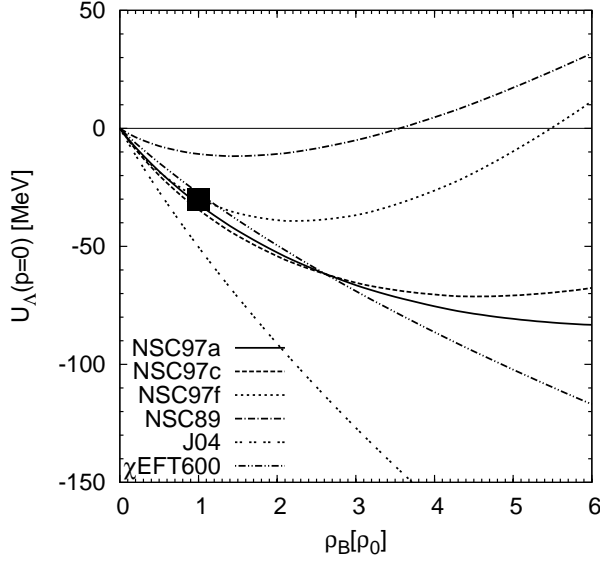


FIG. 6: $U_\Lambda(p=0)$ as a function of density in symmetric nuclear matter. The square represents the empirical point $U_\Lambda(p=0) \approx -30$ MeV [32].

The density dependence for several Λ potentials at rest (i.e. $p=0$) in symmetric nuclear matter is compared in Fig. 6. The square represents the generally expected empirical potential depth of $U_\Lambda(p=0) \approx -30$ MeV. This value has been recently confirmed by an analysis of the (π^-, K^+) inclusive spectra on various target nuclei as best fits in a framework of a distorted-wave approximation [32]. While most potentials can reproduce this value, the Jülich potential (J04) yields a stronger binding while the old Nijmegen potential (NSC89) underestimates the binding.

With the exception of the J04 and NSC89 potentials, all others agree up to the saturation density. However, with increasing density, the differences between these potentials grow, leading to different bindings at rest. This will have consequences for the predictions of the Λ hyperon concentration in dense nuclear matter. In particular, this will affect the maximum mass of neutron stars. It is interesting to observe that even the Nijmegen potentials NSC97a-f are different from each other at higher densities, since the only difference between the bare potentials NSC97a-f is the $F/(F+D)$ ratio.

In the past, the potentials NSC89 [33] and NSC97a,f [3] have also been used as a basis for a single-particle potential calculation in the G -matrix formalism. These G -matrix calculations yield a more attractive Λ potential. For example, at saturation density a potential depth of -29.8 MeV is found for the NSC89 potential, the NSC97a gives -39.7 MeV, and the NSC97f -36.6 MeV. On the other hand, a comparison with another G -matrix calculation [4], which uses a different prescription for intermediate state spectra, yields similar results to ours.

In Fig. 7 the momentum dependence of the Λ potential

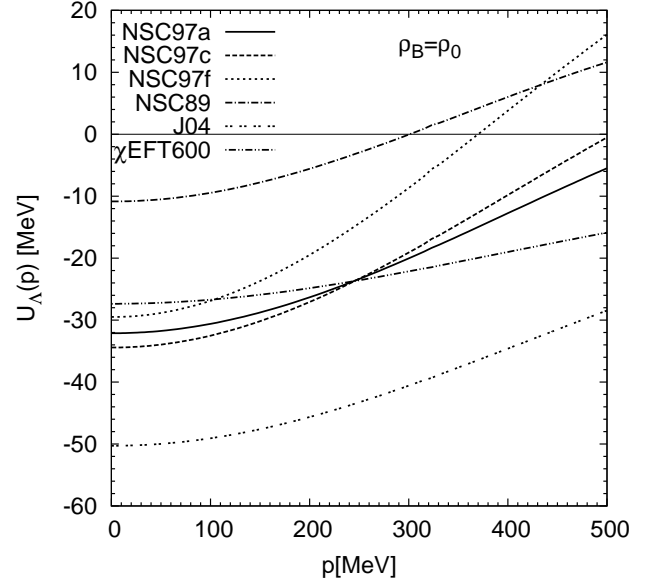


FIG. 7: Momentum dependence of $U_\Lambda(p)$ at saturation density in symmetric nuclear matter.

at saturation density for various YN potentials is shown. While all potentials increase with increasing momentum, the slopes deviate of each other. Similar differences in the momentum behavior of the single-particle potentials are also seen in other works, cf. e.g. [33, 34].

	1S_0	3S_1	1P_1	3P_0	3P_1	3P_2	3D_1	U_Λ
NSC97a	-4.86	-27.79	1.70	-0.10	2.10	-2.03	-0.09	-32.12
NSC97b	-6.69	-27.40	1.86	0.05	2.53	-1.87	-0.09	-32.72
NSC97c	-9.06	-27.54	1.96	0.36	2.84	-1.72	-0.09	-34.42
NSC97d	-12.14	-26.05	2.22	0.64	3.54	-1.33	-0.08	-34.46
NSC97e	-13.92	-24.43	2.43	0.75	4.09	-1.03	-0.07	-33.50
NSC97f	-15.37	-20.85	2.85	0.68	5.09	-0.47	-0.05	-29.49
NSC89	-15.73	4.52	2.00	0.52	2.55	-3.46	-0.07	-10.84
J04	-9.55	-35.18	-0.15	-0.70	0.58	-3.17	-1.31	-50.28
χEFT550	-11.11	-15.46	1.50	-1.69	3.17	-0.07	-3.14	-27.14
χEFT600	-12.29	-11.39	1.50	-1.73	3.17	-0.07	-6.14	-27.37
χEFT650	-11.99	-6.70	1.50	-1.77	3.17	-0.07	-9.90	-26.27
χEFT700	-11.91	-1.77	1.50	-1.81	3.17	-0.08	-13.84	-25.35

TABLE III: Partial wave contributions to the Λ potential $U_\Lambda(p=0)$ at $\rho_B = \rho_0$ in symmetric nuclear matter.

In addition, Eq. (7) cannot only be used for the calculation of $U_Y(p)$, but also to extract the individual partial-wave contributions to the total potential. These contributions are obtained by neglecting the summation over the LSJ quantum numbers in Eq. (7), which we label in the following as $U_Y(^{2S+1}L_J)$. In Tab. III and Tab. IV the resulting partial-wave contributions to U_Λ and U_{Σ^-} , respectively, are listed for several YN interactions at van-

ishing momenta at saturation density.

	1S_0	3S_1	1P_1	3P_0	3P_1	3P_2	3D_1	U_{Σ^-}
NSC97a	3.51	-4.87	-2.16	0.59	1.46	-2.41	-0.01	-4.73
NSC97b	3.58	-5.37	-2.14	0.63	1.54	-2.31	-0.01	-4.91
NSC97c	3.48	-6.50	-2.12	0.68	1.59	-2.18	0.00	-5.86
NSC97d	3.50	-6.08	-2.02	0.71	1.70	-1.92	0.01	-4.88
NSC97e	3.50	-5.24	-1.94	0.72	1.78	-1.75	0.02	-3.65
NSC97f	3.51	-5.11	-1.85	0.71	1.90	-1.60	0.02	-3.14
NSC89	-4.32	11.46	-0.77	0.93	2.27	-1.49	0.28	7.61
J04	-7.63	1.84	-0.15	0.52	-0.70	-3.37	-3.65	-15.13
χ EFT550	2.28	14.69	1.50	-0.20	0.09	-0.01	-2.73	14.11
χ EFT600	-3.70	66.26	1.50	-0.28	0.06	-0.01	-5.36	56.89
χ EFT650	-2.72	42.41	1.50	-0.35	0.01	-0.01	-8.60	30.38
χ EFT700	-2.93	39.93	1.50	-0.41	-0.04	-0.02	-11.60	24.68

TABLE IV: Partial-wave contributions to the Σ^- single-particle potential $U_{\Sigma^-}(p=0)$ at $\rho_B = \rho_0$.

In these tables the partial waves up to $L = 2$ are shown and the last column contains the sum up to $L = 5$. As expected, the influence of the S - and D -waves is the most dominant one. One can see that the combination of the coupled 3S_1 and 3D_1 channels provides most of the attraction in the majority of the Λ potentials.

These tables also illustrate the different contributions to the hyperon potentials originating from the central, spin-spin, spin-orbit parts of the YN interaction. These partial waves can then be used to determine the size of these contributions, which could then be compared to other results such as [4, 35, 36, 37]. Furthermore, one can recognize that a change in the $F/(F+D)$ ratio from the different bare NSC97a-f potentials affects U_Λ stronger than the U_{Σ^-} .

Another interesting feature is that the χ EFT successfully reproduces the potential depth at saturation density. For these densities, the χ EFT agrees well with the Nijmegen NSC97a-f potentials. Fig. 8 shows a comparison of the $U_\Lambda(p=0)$ density dependence, obtained with the χ EFT, with results from [37]. Perfect agreement for the $U_\Lambda(p=0)$ is evident and the independence of the χ EFT potential on the regulator cutoff is also seen. This suggests that the two approaches in Refs. [38] and [37] to construct an χ EFT, are closely related. Furthermore, χ EFT in leading order can already produce a reasonable ΛN potential.

Fig. 9 shows the density dependence for several Σ^- potentials at rest in symmetric nuclear matter similar to the previous figure. The other members of the Σ triplet, Σ^+ and Σ^0 , exhibit an almost identical behavior. A small difference compared to the Σ^- case is found to be due to a small difference in their masses. Therefore, in the remaining section we discuss only the Σ^- potential. For U_{Σ^-} no density range is found where all or even most potentials agree. However, the difference between the

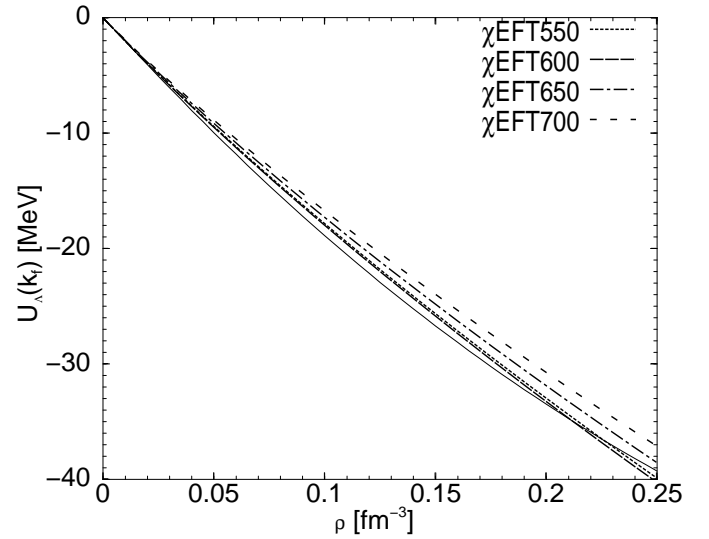


FIG. 8: Density dependence of $U_\Lambda(p=0)$ for symmetric nuclear matter, $\rho = 2k_F^3/3\pi^2$. Full lines are from [37] and dashed lines represent χ EFT for various regulator cutoffs.

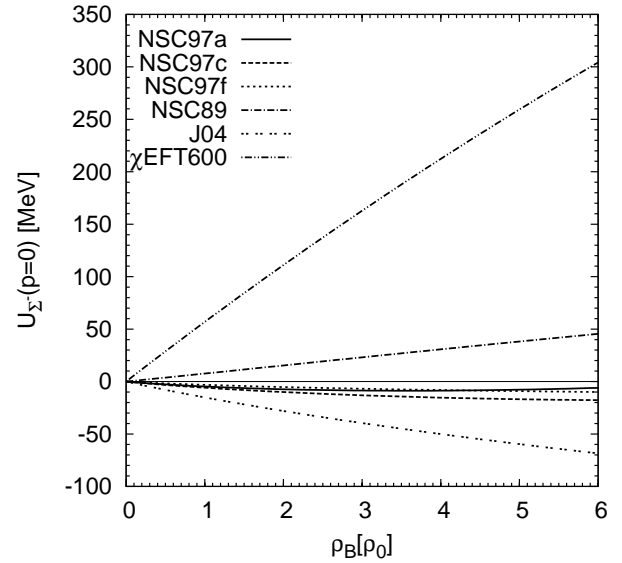


FIG. 9: Similar to Fig. 6 for the $U_{\Sigma^-}(p=0)$.

NSC97a-f potentials is not significant and is the same over the entire range of densities shown. This further confirms that the influence of the $F/(F+D)$ ratio on the ΣN interaction is less important than on ΛN . Due to experimental uncertainties in case of the Σ potential, no generally accepted empirical point can be used as a reference. On the one hand, recent results [32], based on the distorted-wave impulse approximation, yield a repulsive potential of the order of 100 MeV. On the other hand, the analysis of the same data by [39] in a semiclassical distorted-wave model and an analysis by [40] within a distorted-wave impulse approximation with a local optimal Fermi averaged T -matrix find a less repulsive poten-

tial. In addition, there exists a bound state of ${}^4_\Sigma\text{He}$ [41], which definitely requires an attractive potential. Thus, for this case no conclusive answer on the theoretical as well as experimental side can be given.

Compared with a G -matrix calculation a stronger binding for the Σ single particle potential is found. In particular, using the NSC89 interaction a binding of -15.3 MeV [33] is found while for the NSC97a potential -29.7 MeV and for the NSC97f potential -25.5 MeV are reported [3]. In order to understand the origin of such a significant difference the individual partial-wave contributions to the potential by [33] are compared with each other. The 1S_0 channel contributions are approximately the same while those for the 3S_1 channel are significantly different.

This difference in the 3S_1 channel is present for both Λ and Σ^- potentials and is the results of the difference in the treatment of the 3S_1 $\Lambda N - \Sigma N$ channel. Since the effective interactions are constructed from $V_{\text{low } k}$ and the G -matrix formalisms, respectively, the difference comes from the treatment of the attractive part of the bare potentials above the cutoff. This is similar to the point made in Fig. 2 where a cutoff dependence is visible: by lowering the cutoff more and more 'attraction' is effectively added to the interaction. It is also interesting to note, that the effective potentials constructed in the G -matrix calculations, NSC89 and NSC97a,f depend on the underlying bare potentials in a similar way as the potentials shown here. This is another sign that the uncertainties are inherent in the underlying potentials.

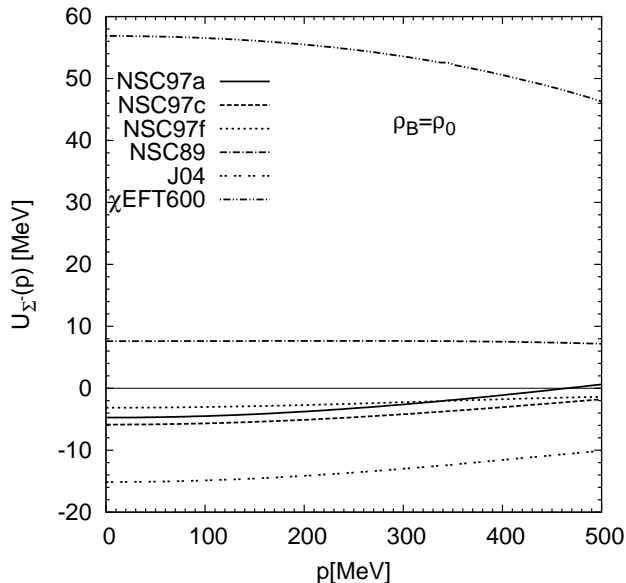


FIG. 10: Similar to Fig. 7 for $U_{\Sigma^-}(p)$.

In Fig. 10 the momentum dependence of the U_{Σ^-} at saturation density for various YN potentials is displayed and illustrates how strongly the results depend on the parameterization of the YN interaction and reiterates that the ΣN interaction is very poorly constrained.

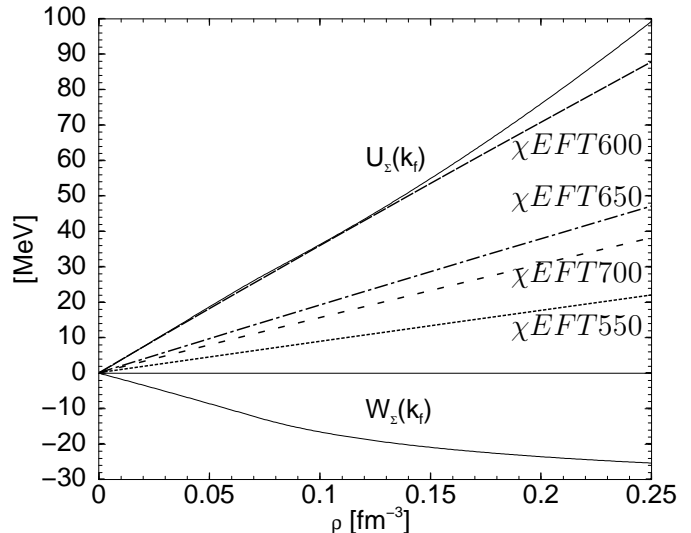


FIG. 11: Density dependence of $U_{\Sigma}(p=0)$ for symmetric nuclear matter. The full line comes from [35] and the dashed lines represent χ EFT results for various values of the regulator cutoff.

Fig. 11 shows the density dependence of the real part $U_{\Sigma}(p=0)$ and the imaginary $W_{\Sigma}(p=0)$ of an optical potential calculation of Ref. [35] together with the results obtained from χ EFT. The most interesting feature here is that all potentials are positive and grow with increasing density in contrast to other potentials. However, unlike in the case of the Λ potential, U_{Σ^-} depends on the regulator cutoff and only χ EFT with a cutoff of 600 MeV agrees with the results of Ref. [35] quantitatively. As already mentioned earlier, the repulsive Σ^- potential, which grows with density, has been suggested by Saha et al. [32] by means of an analysis of (π^-, K^+) inclusive spectra.

Recently, a calculation of the binding energy of the Λ hyperon in nuclear matter within a Dirac-Brueckner-Hartree-Fock framework was performed using the most recent Jülich meson exchange YN potential [42]. The reported values of the Λ potential of -51.27 MeV (-47.4 MeV) in Brueckner-Hartree-Fock (Dirac-Brueckner-Hartree-Fock) framework agree well with our prediction of -50.28 MeV.

IV. SUMMARY AND CONCLUSIONS

In this paper an application of recently constructed YN $V_{\text{low } k}$ potentials [8, 9] is presented. The potentials were constructed in a RG formalism and applied to nuclear matter. The calculation of the single-particle potential of the Λ and Σ hyperon was performed in the Hartree-Fock approximation. Since the $V_{\text{low } k}$ is a low-momentum interaction, it can be directly used in the considered range of momenta.

For comparison with other approaches, scattering lengths and the single-particle potential of several bare

potentials were calculated. In contrast to the NN case, it is not possible to obtain a precise fit of the YN potential to all partial waves, due to the incomplete YN scattering data base. This deficiency is clearly visible in the results obtained.

A few interesting observations are in order, however. The $V_{\text{low } k}$ for the $\Sigma^- N \ ^1S_0$ channel is cutoff independent in between momenta of 250 and 500 MeV, but no such independence was found in the 3S_1 channel due to a strongly attractive short-range part. The results for the Λ potential are more satisfying since most of the potentials agree up to saturation density and reproduce the empirical point. An interesting observation is that χEFT in leading order lies among these potentials. However, for the Σ^- potential no such agreement exists. Unfortunately, the present experimental situation for Σ^- does not allow for more stringent conclusions.

Finally, the results are also compared with other approaches, [4, 33, 34]. Most of the results of a G -matrix calculations yield a stronger binding than we find. The difference comes from the way in which the attraction, es-

pecially in the $\Sigma N \rightarrow \Lambda N$ channels, is treated in the RG approach. In comparison with χEFT overall agreement is seen [35, 37].

However, the most interesting fact is that differences in approaches, $V_{\text{low } k}$, G -matrix and χEFT , are much less than the differences between the various potentials. Thus the differences we see here are not the result of the approaches used to construct the effective interaction, but largely reflect uncertainties in the underlying bare potentials.

Acknowledgments

This work has been partially supported by the Helmholtz Gemeinschaft, program Grant No. VH-VI-041 and by the Helmholtz Research School for Quark Matter Studies. We would like to thank Mathias Wagner and Isaac Vidaña for useful discussions.

-
- [1] A. Gal, Prog. Theor. Phys. Suppl. **156**, 1 (2006).
 - [2] M. Kohno, Y. Fujiwara, T. Fujita, C. Nakamoto, and Y. Suzuki, Nucl. Phys. **A674**, 229 (2000).
 - [3] I. Vidana, A. Polls, A. Ramos, and H.-J. Schulze, Phys. Rev. **C64**, 044301 (2001).
 - [4] T. A. Rijken, V. G. J. Stoks, and Y. Yamamoto, Phys. Rev. **C59**, 21 (1999).
 - [5] S. R. Beane et al., hep-lat/0612026.
 - [6] S. R. Beane, P. F. Bedaque, A. Parreno, and M. J. Savage, Nucl. Phys. **A747**, 55 (2005).
 - [7] S. K. Bogner, T. T. S. Kuo, and A. Schwenk, Phys. Rept. **386**, 1 (2003).
 - [8] M. Wagner, B.-J. Schaefer, J. Wambach, T. T. S. Kuo, and G. E. Brown, Phys. Rev. **C74**, 054003 (2006).
 - [9] B.-J. Schaefer, M. Wagner, J. Wambach, T. T. S. Kuo, and G. E. Brown, Phys. Rev. **C73**, 011001 (2006).
 - [10] H. Polinder, J. Haidenbauer, and U. G. Meissner, Phys. Lett. B **653**, 29 (2007), arXiv:0705.3753 [nucl-th].
 - [11] K. Suzuki and S. Y. Lee, Prog. Theor. Phys. **64**, 2091 (1980).
 - [12] K. Suzuki and S. Y. Lee, Phys. Lett. **B91**, 173 (1980).
 - [13] F. Andreozzi, Phys. Rev. **C54**, 684 (1996).
 - [14] P. M. M. Maessen, T. A. Rijken, and J. J. de Swart, Phys. Rev. **C40**, 2226 (1989).
 - [15] J. Haidenbauer and U.-G. Meißner, Phys. Rev. **C72**, 044005 (2005).
 - [16] B. Holzenkamp, K. Holinde, and J. Speth, Nucl. Phys. **A500**, 485 (1989).
 - [17] A. Reuber, K. Holinde, and J. Speth, Nucl. Phys. **A570**, 543 (1994).
 - [18] T. A. Rijken and Y. Yamamoto, nucl-th/0608074,
 - [19] T. A. Rijken and Y. Yamamoto, Phys. Rev. **C73**, 044008 (2006).
 - [20] L. Micu, Nucl. Phys. **B10**, 521 (1969).
 - [21] P. F. Bedaque and U. van Kolck, Annu. Rev. Nucl. Part. Sci. **52**, 339 (2002).
 - [22] E. Epelbaum, Prog. Part. Nucl. Phys. **57**, 654 (2006).
 - [23] R. J. Furnstahl, G. Rupak, and T. Schaefer, arXiv:0801.0729 [nucl-th],
 - [24] S. Weinberg, Phys. Lett. **B251**, 288 (1990).
 - [25] S. Weinberg, Nucl. Phys. **B363**, 3 (1991).
 - [26] E. Epelbaum, W. Glöckle, and U.-G. Meissner, Nucl. Phys. **A747**, 362 (2005).
 - [27] H. Polinder, J. Haidenbauer, and U.-G. Meißner, Nucl. Phys. **A779**, 244 (2006).
 - [28] C. L. Korpa, A. E. L. Dieperink, and R. G. E. Timmermans, Phys. Rev. **C65**, 015208 (2002).
 - [29] J. Haidenbauer, U.-G. Meissner, A. Nogga, and H. Polinder, Lect. Notes Phys. **724**, 113 (2007).
 - [30] D. B. Kaplan, M. J. Savage, and M. B. Wise, Nucl. Phys. **B534**, 329 (1998).
 - [31] A. L. Fetter and J. D. Walecka, *Quantum Theory Of Many-particle Systems* (McGraw-Hill, Inc., 1971).
 - [32] P. Saha et al., Phys. Rev. **C70**, 044613 (2004).
 - [33] H.-J. Schulze, M. Baldo, U. Lombardo, J. Cugon, and A. Lejeune, Phys. Rev. **C57**, 704 (1998).
 - [34] I. Vidana, I. Bombaci, A. Polls, and A. Ramos, Astron. Astrophys. **399**, 687 (2003).
 - [35] N. Kaiser, Phys. Rev. **C71**, 068201 (2005).
 - [36] H. J. Pirner, Phys. Lett. **B85**, 190 (1979).
 - [37] N. Kaiser and W. Weise, Phys. Rev. **C71**, 015203 (2005).
 - [38] H. Polinder, Ph.D. thesis, Nijmegen (2004).
 - [39] M. Kohno, Y. Fujiwara, Y. Watanabe, K. Ogata, and M. Kawai, Phys. Rev. **C74**, 064613 (2006).
 - [40] H. Maekawa, K. Tsubakihara, and A. Ohnishi, nucl-th/0701066.
 - [41] T. Nagae et al., Phys. Rev. Lett. **80**, 1605 (1998).
 - [42] F. Sammarruca, arXiv:0801.0879 [nucl-th],